# Shear wave focusing for three-dimensional sonoelastography

Zhe Wu and Lawrence S. Taylor
*Department of Electrical and Computer Engineering, University of Rochester, Rochester, New York 14627*

Deborah J. Rubens
*Department of Radiology, University of Rochester Medical Center, Rochester, New York 14627*

Kevin J. Parker
*Department of Electrical and Computer Engineering, University of Rochester Medical Center, Rochester, New York 14627*

(Received 4 April 2001; accepted for publication 20 September 2001)

A new vibration scheme is shown to provide localized vibration fields for three-dimensional sonoelastography imaging. The theoretical vibration distributions of double strip loads vibrating normally to the surface of a semi-infinite elastic space are calculated. A localization or focusing of shear waves inbetween the double-strip loads is predicted. Experimentally, two parallel rigid rectangular cross-section bars are mounted on an electromagnetic shaker. Driven by the signal source, the bars vibrate against the surface of a tissue-mimicking phantom. The double-bar source is also used to propagate shear wave into an *ex vivo* prostate phantom with a 6 mm ''tumor'' in it. A combination of high frequencies (400–600 Hz) is used to drive the double-bar applicator. In the phantom experiments, a shear wave focal zone with higher vibration amplitude and uniformity predicted by the theory was confirmed. The position of the focal zone is controllable when adjusting the separation of the bars as the theory shows. When this vibration scheme was used in a prostate phantom experiment, high-resolution tumor images with clear boundaries are obtained. The parallel bar is an ideal applicator to create more uniform vibration within a controllable localized volume. The field has uniformity especially in the direction along the bars. © *2002 Acoustical Society of America.* [DOI: 10.1121/1.1419093]

PACS numbers: 43.80.Cs, 43.80.Ev [FD]

## I. INTRODUCTION

Low frequency shear waves can be used to reveal the mechanical properties of soft tissues and thus to detect and quantify hard lesions in the body (Parker *et al.*, 1990; Yamakoshi *et al.*, 1990). Since the three-dimensional (3D) tumor visualization and the measurement of the tumor volume are important in many cases (Egevad *et al.*, 1998), 3D sonoelastography is of great interest.

3D sonoelastography (Taylor *et al.*, 2000) is a technique that images hard lesions by acquiring a sequence of two-dimensional (2D) slices, which are subsequently assembled into a 3D volume. One of the challenges of this technique is to create a relatively uniform vibration field throughout the 3D region of interest. In sonoelastography, the lesion is detected by the local decrease in vibration amplitude caused by a hard (high shear modulus) lesion relative to the higher vibration in the softer (low shear modulus), surrounding tissue. In addition to direct imaging of vibration shear wave fields, it is also possible to estimate local values of Young's modulus within the regions of interest (Fu *et al.*, 2000).

The shear wave fields propagated in tissue are greatly influenced by the type of source that is employed. Yamakoshi *et al.* (1990) used a rectangular plate (20 mm by 60 mm) when using forced low frequency vibration to propagate shear waves in tissue phantoms. The vibration was normal to the surface of the phantom and the resulting vibration field was uniform along the longer side of the plate. Fu *et al.* (2000) later used a long rigid bar with a smaller rectangular cross section to create a plane-strain vibration field for reconstruction of the Young's modulus of a tissue phantom. The bar was mounted on a rigid column then driven normally to the phantom surface to create a plane strain state. Tanter *et al.* (2000) proposed a system for focusing shear waves for transient elastography imaging in which two bars with circular cross sections were placed beside the ultrasound transducer. Using this system on tissue phantoms they found that larger displacements were generated and shear waves penetrated deeper into the medium.

In this paper we show through theory developed by Miller and Pursey (1954) that the thin rectangular cross section bar (called a ''strip load'') of Fu *et al.* produces a beam pattern with a distinctive ''V'' shape. We then extend the analysis to the parallel-rod configuration employed by Tanter *et al.* and demonstrate how this presents a practical configuration for focusing shear waves for 3D image acquisition. The theoretical models are then confirmed by sonoelastography image experiments. To our knowledge, the beam patterns of single-strip load and double-strip load vibration sources have not previously been verified by both theoretical calculation and experimental verification.

In the first part of the paper, we will look at Miller and Pursey's theory. The single-strip load beam pattern is reviewed, and the theory is extended to double-strip loads. In the second part, experimental results on a tissue-mimicking phantom and *ex vivo* prostate phantom are presented. Experi-

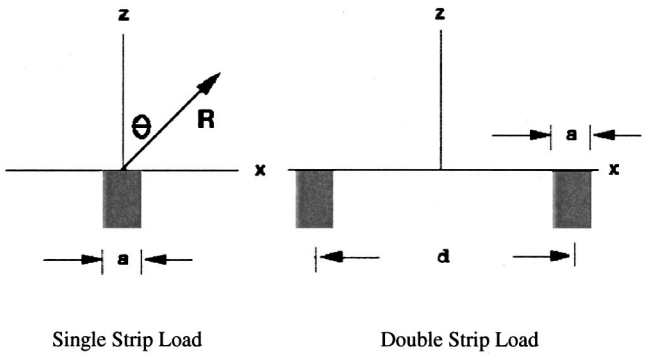


FIG. 1. Image explaining Miller and Pursey's coordinate system for both the single-strip load and the double-strip loads.

ment and theory are shown to agree and confirm that it is possible to create an extended region of shear vibration within elastic materials.

## II. THEORY

Sonoelastography uses propagating shear waves to detect hard lesions surrounded by uniform softer tissues. Since a hard lesion is relatively less compliant to vibration than the soft tissue, localized regions of low vibration in the whole field correspond to the lesions. The vibration field is measured by Doppler ultrasound methods, which can map the peak vibration at any point in real time using the color Doppler mode.

To simulate the vibration field pattern of strip loads, we took advantage of Miller and Pursey's early work on mechanical radiators on an elastic half space in the following two cases.

### A. A strip load with normal vibration

Consider a long thin strip placed in close contact with a semi-infinite large, uniform homogeneous elastic solid and vibrating normal to the surface of the medium (see Fig. 1). The solution for the vibration field in the far field is:

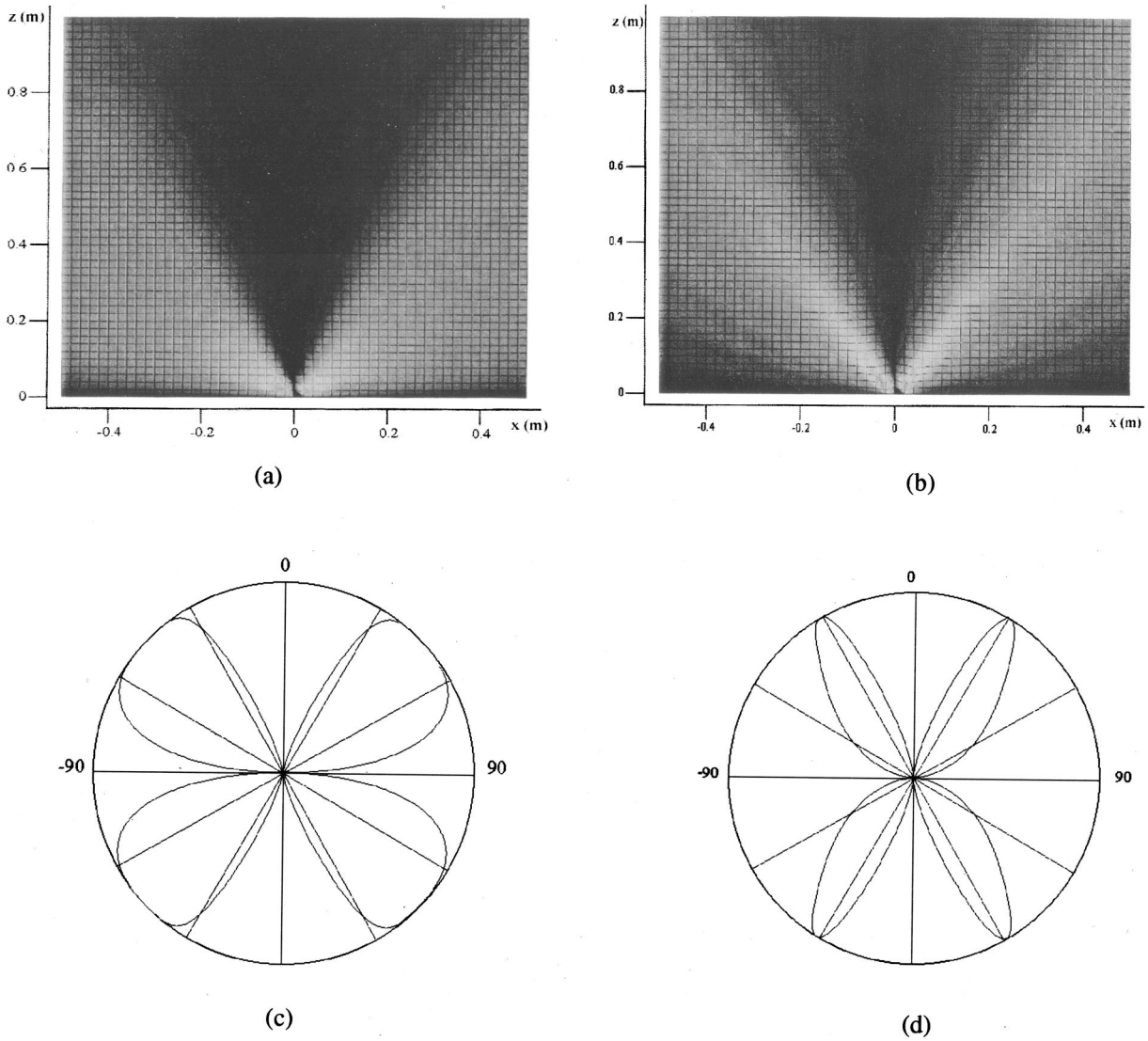


FIG. 2. Vibration fields of the single-strip shaking normal to the medium surface. (a) is *Z* direction field pattern and (b) is *x* direction field pattern. (c) is the angular distribution of $u_z$. (d) is the angular distribution of $u_x$.

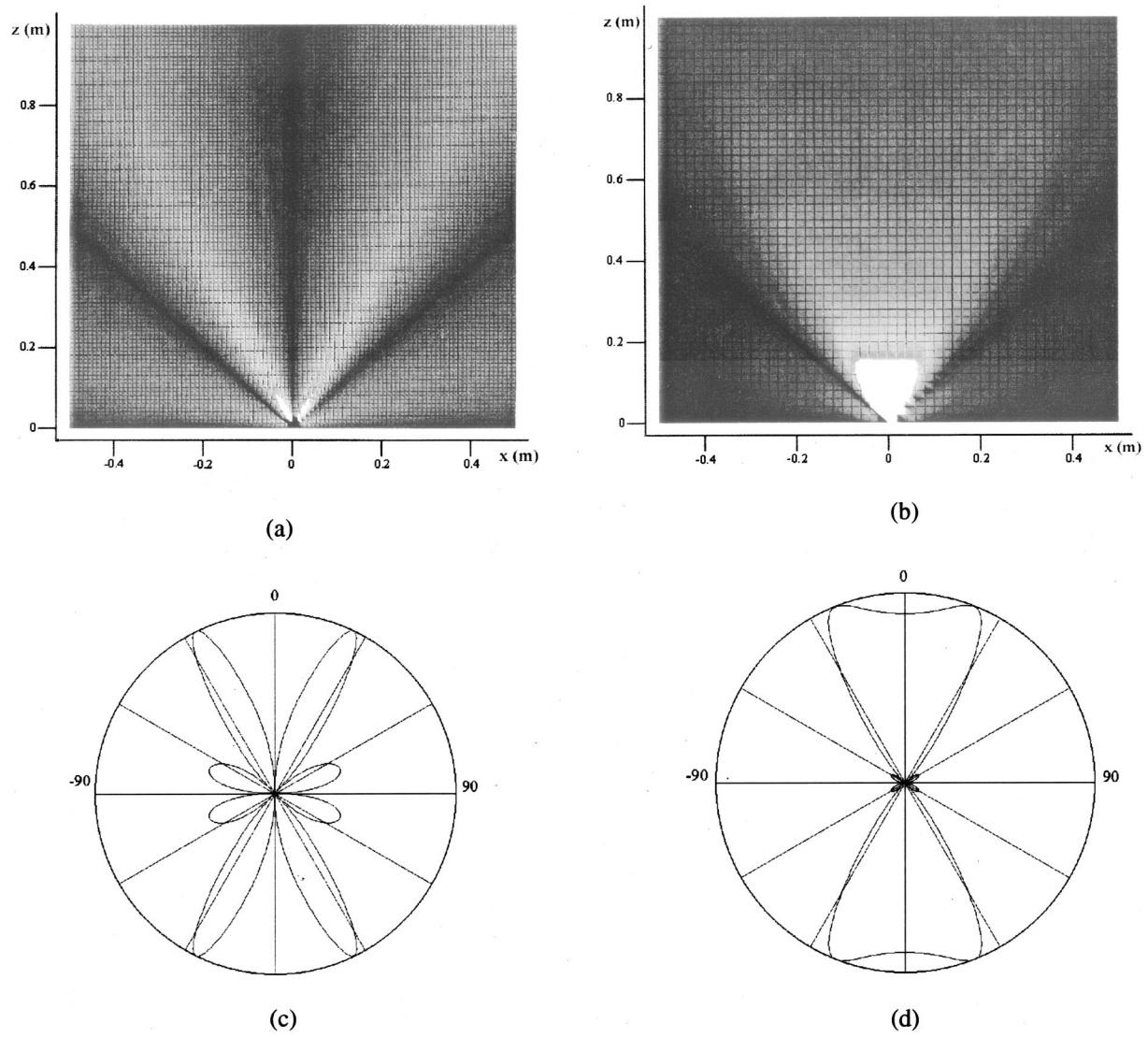


FIG. 3. Vibration fields of single-strip shaking tangential to the medium surface. (a) is the *Z*-direction field pattern, (b) is the *x*-direction field pattern, (c) is the angular distribution of $u_z$, and (d) is the angular distribution of $u_x$.

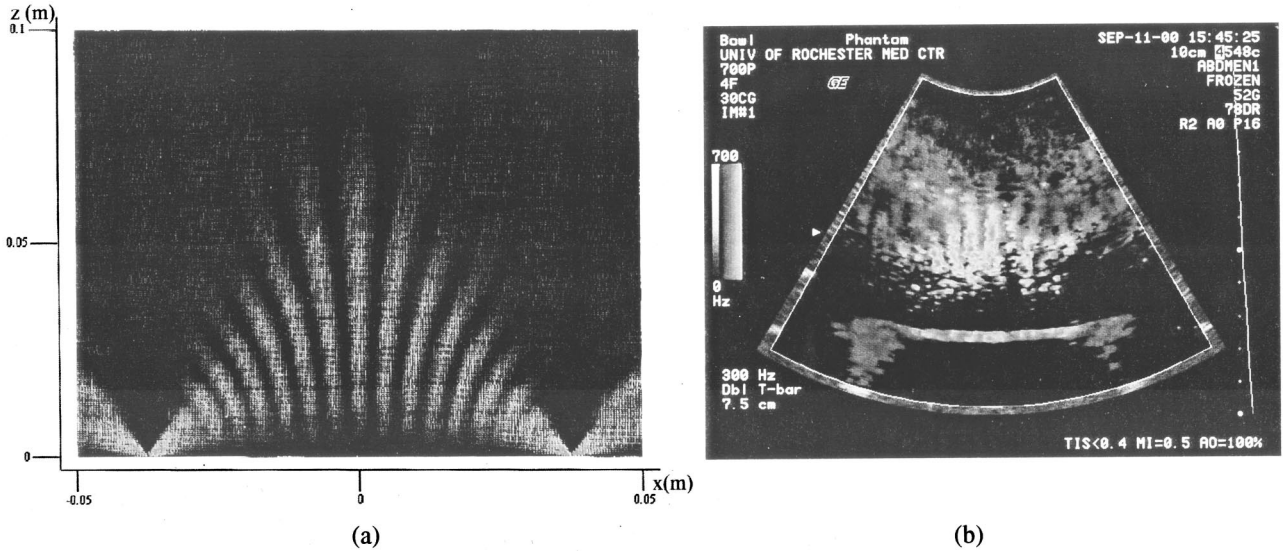


FIG. 4. Double-strip load beam patterns: (a) theoretical calculation of strip loads separated by 75 mm and (b) experiment result taken on Logiq 700. The green horizontal line near the bottom of (b) is the lower surface of the phantom.

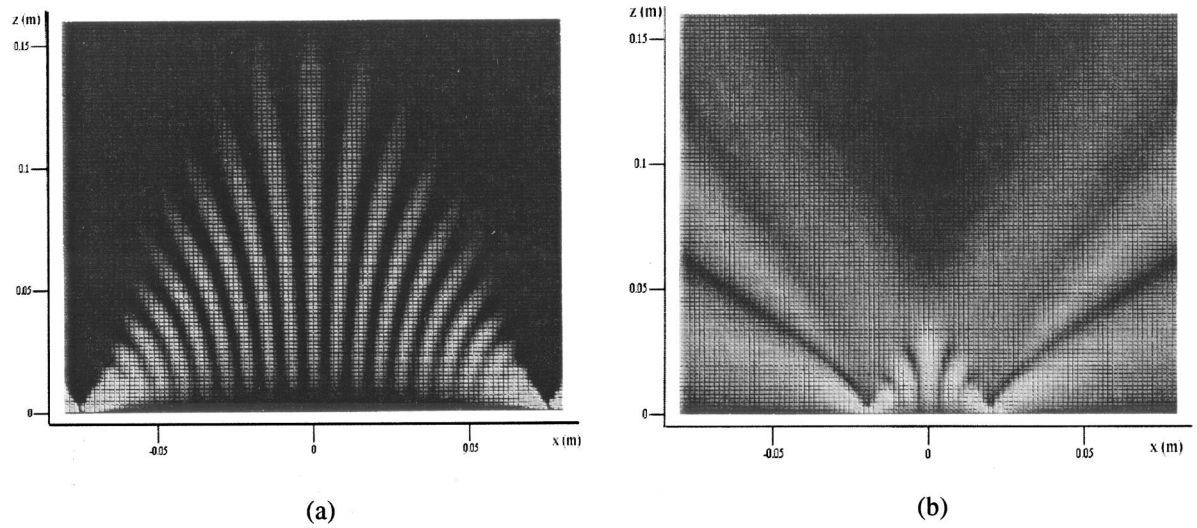


FIG. 5. Patterns change with separation: (a) separation between the two bars is 150 mm, and (b) separation between the two bars is 40 mm.

$$u_z = a \cdot e^{i\pi/4} \cdot \cos\theta \cdot \sqrt{\frac{2}{\pi \cdot R}} \cdot \frac{2\mu^{5/2} \cdot \sin^2\theta \cdot \sqrt{\mu^2 \cdot \sin^2\theta - 1}}{F_0(\mu \cdot \sin\theta)} \cdot e^{-i\mu R} + \frac{i \cdot \cos\theta \cdot (\mu^2 - 2 \cdot \sin^2\theta)}{F_0(\sin\theta)} \cdot e^{-iR}, \quad (1)$$

$$u_x = a \cdot e^{i\pi/4} \cdot \cos\theta \cdot \sqrt{\frac{2}{\pi \cdot R}} \cdot \frac{-\mu^{5/2} \cdot \sin 2\theta \cdot \sqrt{\mu^2 \cdot \sin^2\theta - 1}}{F_0(\mu \cdot \sin\theta)} \cdot e^{-i\mu R} + \frac{i \cdot \sin\theta \cdot (\mu^2 - 2 \cdot \sin^2\theta)}{F_0(\sin\theta)} \cdot e^{-iR}, \quad (2)$$

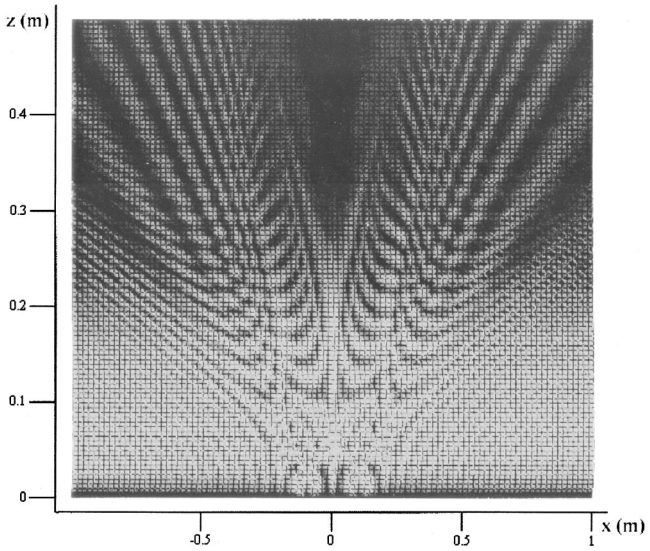


FIG. 6. Side view of the four-strip load beam pattern. From the image, we find a strong vibration region exists in the center of the four-strip load. It is highly focused (refer to the thin pencil-like pattern in the middle) within 20 cm from the load plane.

where $u_z$ is the vibration amplitute in $z$ direction, $u_x$ is the vibration amplitute in the $x$ direction. $a$ is the width of the strip load, $\theta$ is the angle from the normal direction, and $R$ is the distance from the origin. $F_0$ is defined as: $F_0 = (2x^2 - \mu^2)^2 - 4x^2 \cdot \sqrt{(x^2-1) \cdot (x^2 - \mu^2)}$; $\mu = (c_{11}/c_{44})$; $c_{11}$ is the bulk modulus and the $c_{44}$ is the shear modulus.

### B. Tangential excitation

Consider a long thin strip placed in close contact with a semi-infinite large, uniform homogeneous elastic solid and vibrating tangentially to the surface of the medium. In this case:

$$u_z = a \cdot e^{i(3\pi/4)} \cdot \cos\theta \cdot \sqrt{\frac{2}{\pi \cdot R}} \cdot \frac{-\mu^{7/2} \cdot \sin\theta \cdot \cos 2\theta}{F_0(\mu \cdot \sin\theta)} \cdot e^{-i\mu R} + \frac{\sin 2\theta \cdot \sqrt{\mu^2 - \sin^2\theta)}}{F_0(\sin\theta)} \cdot e^{-iR}, \quad (3)$$

$$u_x = a \cdot e^{i(3\pi/4)} \cdot \cos\theta \cdot \sqrt{\frac{2}{\pi \cdot R}} \cdot \frac{\mu^{7/2} \cdot \cos\theta \cdot \cos 2\theta}{F_0(\mu \cdot \sin\theta)} \cdot e^{-i\mu R} + \frac{2\sin^2\theta \cdot \sqrt{\mu^2 - 2 \cdot \sin^2\theta}}{F_0(\sin\theta)} \cdot e^{-iR}. \quad (4)$$

#### *1. Waves separation*

It is clear that Miller and Pursey's solution consists of two terms that travel at different velocities; one wave speed being $\mu$ times larger than the other. Our interpretation is that the faster one is a compressional wave and the slower one is a shear wave. To verify this, we examined the divergence of the slow traveling wave component and the curl of the faster component. In numerical assessments, they are both significantly close to zero, which agrees with the definitions of both types of waves.

We then neglect the compressional wave for the following two reasons. First, the wavelength of the compressional wave is typically as long as a few meters, which is not useful in resolving the lesions or other structures and cannot be supported in small centimeter sized organs. Second, since the

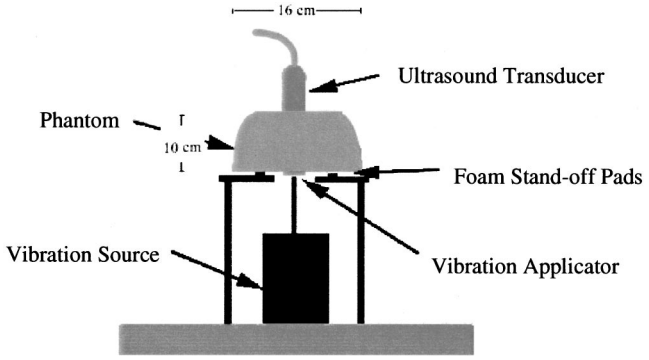


FIG. 7. Experimental setup for acquisition of the vibration images.

bulk modulus is nearly 1000 times larger than the shear modulus (Sarvazyan, 1995) in soft glandular tissue, the amplitude of the compressional wave is actually very small and thus has little contribution to the total pattern.

So, for a normal vibration strip source, the $z$ component and the $x$ component of the shear wave is:

$$u_z = a \cdot e^{i\pi/4} \cdot \cos\theta \cdot \sqrt{\frac{2}{\pi \cdot R}} \cdot \frac{2\mu^{5/2} \cdot \sin^2\theta \cdot \sqrt{\mu^2 \cdot \sin^2\theta - 1}}{F_0(\mu \cdot \sin\theta)} \cdot e^{-i\mu R}, \tag{5}$$

$$u_x = a \cdot e^{i\pi/4} \cdot \cos\theta \cdot \sqrt{\frac{2}{\pi \cdot R}} \cdot \frac{-\mu^{5/2} \cdot \sin 2\theta \cdot \sqrt{\mu^2 \cdot \sin^2\theta - 1}}{F_0(\mu \cdot \sin\theta)} \cdot e^{-i\mu R}. \tag{6}$$

For the tangential excitation strip source, the $z$ component and the $x$ component of the shear wave is:

$$u_z = a \cdot e^{i(3\pi/4)} \cdot \cos\theta \cdot \sqrt{\frac{2}{\pi \cdot R}} \cdot \frac{-\mu^{7/2} \cdot \sin\theta \cdot \cos 2\theta}{F_0(\mu \cdot \sin\theta)} \cdot e^{-i\mu R}, \tag{7}$$

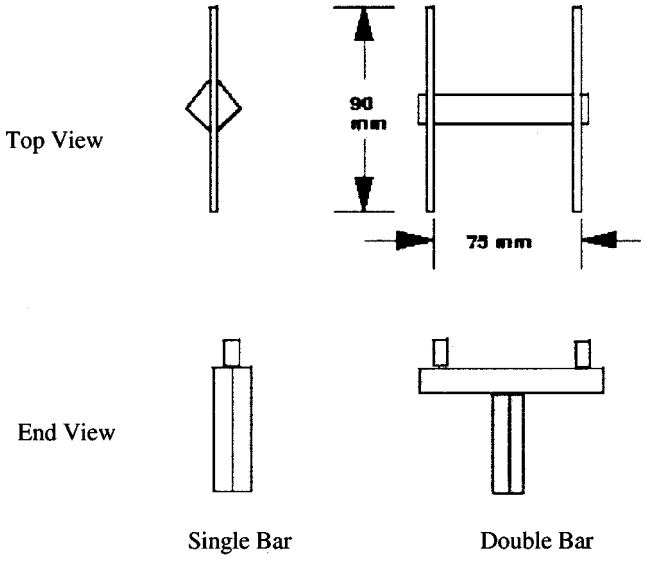


FIG. 8. Sketches and dimension of applicators used in the experiments.

$$u_x = a \cdot e^{i(3\pi/4)} \cdot \cos\theta \cdot \sqrt{\frac{2}{\pi \cdot R}} \cdot \frac{\mu^{7/2} \cdot \cos\theta \cdot \cos 2\theta}{F_0(\mu \cdot \sin\theta)} \cdot e^{-i\mu R}. \tag{8}$$

We plot the beam pattern and directivity functions of the propagating shear wave for both the normal source and the tangential source; see Figs. 2 and 3. One of the interesting features of the pattern is that the angular distribution of the vibration is frequency independent. This effect is observed in the experiments.

### 2. Superposition of strip loads

We next analyze a superposition of the vibration field created by two strip loads placed side by side with a separation of certain distance D. The left branch of the right strip load and the right branch of the left strip load interfere with each other and localize the energy into a small region (Fig. 4). Note that the beam pattern of the double-strip load is related to the wavelength of the propagating shear waves. In theory this provides us with an experimental method to measure the shear wave velocity in the material. The shear modulus can be further obtained from these values, although details of this are beyond the scope of this paper.

Theoretical simulations show the size of the focusing zone is dependent on the separation of the two strips. It can be roughly divided into two ranges. When the separation is large [150 mm as shown in Fig. 5(a)], the focal zone is a triangle located in between the two bars. As the separation reduces to 40 mm or less [as shown in Fig. 5(b)], the focal zone gradually becomes something more like the beam pattern of a single bar, which radiates energy mainly into a V-shape region. The focusing effect is no longer pronounced.

A further extension leads us to a four-strip load placed in a rectangular shape on a plane. All of the strips are infinitely long. As we expect, a region of higher vibration exists along the center axis of the four-strip load if they vibrate normal to their plane in-phase. Figure 6 shows the side view of the beam pattern of a four-strip load. The sharp, pencil-like pattern in the center of the image implies a highly focused vibration field along the center axis, along with an extended lateral region of high vibration.

## III. MATERIALS AND METHODS

A Zerdine tissue phantom (CIRS: Norfolk, VA) was used for the experimental verification of the theory. The tissue-mimicking material has a sound speed near 1540 m/s, a Young's modulus of 20 KPa, and a shear modulus of 6.67 KPa. The phantom is bowl shaped with dimensions as shown in Fig. 7.

With the exception of a few small spherical inclusions in a different region, the phantom is isotropic and homogeneous with a uniform shear modulus. Samples of the phantom material were compression tested and the relaxation phenomenon observed indicated that the material has low shear viscosity. The resulting damping at high frequencies (above 300 Hz) insured that the displacement at the distal boundary of the phantom would be very small, so the bowl phantom is a good simulation of the semi-infinite space. Miller–Pursey

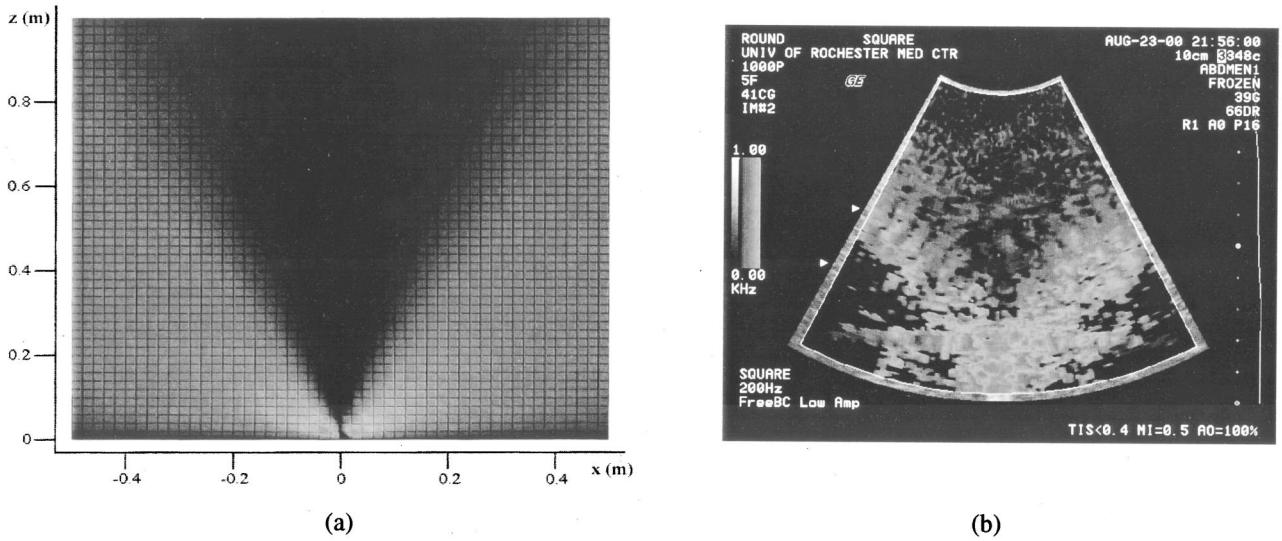


FIG. 9. Single-strip load beam patterns. (a) Theoretical calculation remapped into ultrasound curvilinear probe coordinates. The gray scale is also adjusted according to the digital filters used on the ultrasound machine. (b) Experimental result, taken on GE Logiq 700.

modeled the elastic half-space with stress-free boundary conditions on the surface. To approximate this condition, vibration was applied from below the phantom that was supported with three or four small pieces of closed cell foam cut into square sections approximately 10 mm thick and 15 mm on each side.

The infinitely long strip load was approximated by a rigid metal strip with a rectangular cross section 90 mm long, 6 mm wide, and 7 mm high supported on a column. The 6 mm edge was applied to the bottom surface of the phantom and driven normally to the phantom surface by a vibration shaker (Vibration Test Systems: Aurora, OH). Power to the shaker was provided by an audio amplifier driven either by a frequency generator when pure tones were used or by a harmonic waveform generator (Model #3511A Pragmatic Instruments: San Diego, CA) when multi-tone frequencies were used. Multi-tone signals were found effective in suppressing the modal patterns resulting from reflections off of the boundaries of the phantom (Taylor *et al.*, 2000). Multi-tone signals used in these experiments were, in our shorthand notation, w22 [200 267 333 400 Hz] with a mean frequency of 338 Hz and w37 [333 400 467 533 Hz] with a mean frequency of 440 Hz. All vibrations were applied as steady-state harmonic signals.

To image the beam pattern, the ultrasound transducer was applied from above, thus orienting the image plane normal to the long axis of the strip load and centering it about 45 mm from each edge. In this configuration, the applied force is a vector parallel to the image plane. A GE Logiq 700 ultrasound machine (GE Medical Systems: Milwaukee, WS) was modified to map Doppler variance to the screen in the color-flow mode. Doppler spectral variance is directly proportional to the square of the peak vibration amplitude (Huang *et al.*, 1990; Taylor *et al.*, 2000). See Figs. 8 and 7 for the experimental setup.

To perform a double-strip load focusing experiment, an

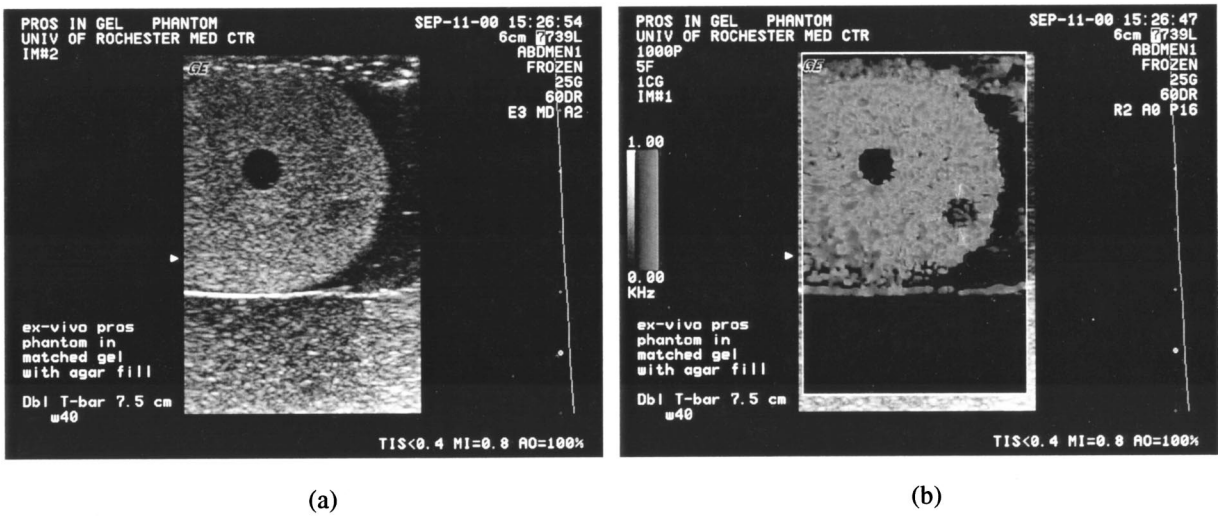


FIG. 10. Sonoelastography image of a prostate phantom with a hard lesion in the lower right quadrant. Double-strip loads are used as a vibration source. Separation between the two bars is 7.5 cm. The tumor size is approximately 6 mm in diameter. The central hole is the urethra-mimicking tube. (a) Conventional B-scan image of the phantom and (b) Sonoelastographic image of the phantom.

applicator was fabricated by mounting two rigid metal strips with a rectangular cross section 90 mm long, 8 mm wide, and 6 mm high in parallel on a rigid metallic bar. The centerline separation between the two parallel strips was adjusted to be 30, 50, or 75 mm.

## IV. EXPERIMENTS AND RESULTS

We first compare the theory to the experiment for the single-strip load. Figure 9(b) shows the experimental beam patterns of single-strip load. We used a pure tone 200 Hz in this experiment. Since the imaging transducer detects vibration in the ''sector scan'' direction of the radiating ultrasound beam, the theoretical pattern is remapped from $X$-$Y$ coordinates into the polar coordinates of the ultrasound probe and presented as a reference. The gray scale, representing the vibration amplitude, is also adjusted to simulate the imaging system response of GE Logiq 700 [Fig. 9(a)] (Taylor *et al.*, 2000).

The theory predicts that the shape of the strip load pattern is frequency independent. To verify this, we ran the frequency generator from 200 Hz to 400 Hz, stepping every 10 Hz. No change of the shape was observed within this range of frequency. A predictable and frequency-independent beam pattern is most useful for sonoelastography. Furthermore, the frequency independent feature of the strip load patterns enables us to apply the multi-frequency signal for reduction of modal artifacts (Taylor *et al.*, 2000).

In the double-strip load experiment, two parallel rigid rectangular cross-section bars with 75 mm separation were used. Driven by the signal source, the bars vibrate against the surface of a tissue-mimicking, bowl-shaped phantom, and a focal zone with higher vibration and uniformity predicted by the theory was confirmed. The position of the focal zone is controllable when adjusting the separation of the bars as the theory shows, as shown in Fig. 5.

The double bar was also used to propagate shear waves into a Zerdine *ex vivo* prostate phantom (CIRS: Norfolk, VA) in which there is a 6 mm ''tumor'' with a Young's modulus approximately seven times that of the surrounding medium. To better simulate the condition inside the body, the prostate phantom was surrounded by a gel phantom with similar elastic properties. A combination of high frequencies (400–600 Hz) is used to drive the double-bar applicator. High-resolution tumor images with clear boundaries are obtained, as shown in Fig. 10.

## V. DISCUSSION

In our experimental studies, the vibrating applicator is typically placed beneath the sample shaking normally to the surface while the ultrasound probe is right above the sample. The ultrasound Doppler scanning principally measures the $Z$ component (i.e., vertical component) of the vibration. For this reason, we are going to mainly discuss the $u_z$ component of the normally shaking source.

Figure 2 shows that a normal vibrating single-strip load propagates shear wave into a V-shaped range. The angle between either branch (of $u_z$) and the normal direction is approximately 45 deg. This agrees very well with the experimental result (Fig. 9).

The shear waves from the double-strip loads meet and interfere inbetween the two loads. The interference effect localizes the energy into a small triangle region (Fig. 4). The height of the triangle is approximately half of the strip load separation. This information enables us to cover the region of interest by adjusting the separation of strip loads.

To verify that the shear wave field of strip loads is uniform along the axes of the strips, we moved the ultrasound probe from one end of the strips to the other, leaving a 1 cm margin on both ends. From the real-time image on the screen, the shape and magnitude of the vibration field appeared to be consistent.

When using a single frequency of vibration, the shear wave field of double-strip loads has some lobe-spacing effect due to spatially constructive and deconstructive interference. This can be eliminated by using multi-frequency signals in sonoelastography experiments where a uniform background is desired.

## VI. CONCLUSION

We have shown through theory and experiments that a double-strip load can focus shear waves, which efficiently produces a stronger vibration field within a controllable region. From the nature of the applicator, the field is reasonably uniform along the strips. These features make double-strip loads a useful applicator for 3D sonoelastography. However, the idealized pattern given by theory and approximated in homogeneous, isotropic phantom experiments will not be realized in tissues. The additional complications of tissue boundaries, along with inhomogeneous and isotropic properties of some tissues, will modify the shear wave patterns. However, the general behavior of the double-strip line provides a useful standing point.

## ACKNOWLEDGMENTS

This work was supported in part by the NSF/NYS Center for Electronic Imaging Systems, NIH grant No. 2 R01 AG16317-01A1, the University of Rochester Department of Radiology and Electrical and Computer Engineering and the General Electric Company (GE). The authors thank GE Medical Systems Division for the loan of the Logiq 700 ultrasound scanner used in the imaging experiments.

Egevad, L., Norberg, M., and Mattson, S. *et al.* (**1998**) ''Estimation of prostate cancer volume by multiple core biopsies before radical prostatectomy,'' Urology **52** (4), 653–658.

Fu, D., Levinson, S., Gracewski, S., and Parker, K. (**2000**). ''Noninvasive quantitative reconstruction of tissue elasticity using an iterative forward approach,'' Phys. Med. Biol. **45**, 1495–1510.

Huang, S. R., Lerner, R. M., and Parker, K. J. (**1990**). ''On estimating the amplitude of harmonic vibrations from the Doppler spectrum of reflected signals,'' J. Acoust. Soc. Am. **88**, 310–317.

Miller, G., and Pursey, H. (**1954**). ''The field and radiation impedance of mechanical radiators on the free surface of a semi-infinite isotropic solid,'' Proc. R. Soc. London, Ser. A **223**, 521–541.

Parker, K. J., Huang, S. R., Musulin, R. A., and Lerner, R. M. (**1990**). ''Tissue response to mechanical vibrations for 'sonoelasticity imaging','' Ultrasound Med. Biol. **16**, 241–246.

Sarvazyan, A. P., Skovoroda, A. R., Emelianov, S. Y., Fowlkes, L. B., Pipe, J. G., Adler, R. S., and Carson, P. L. (**1995**). ''Biophysical bases of elasticity imaging,'' in *Acoustical Imaging* (Plenum, New York), Vol. 21, pp. 223–240.

Tanter, M., Sandrin, L., Catheline, S., and Fink, M. (**1999**). ''Time-resolved 2D pulsed elastography,'' (abstract) Ultrason. Imaging **21**, 286.

Taylor, L. S., Porter, B. C., Rubens, D. J., and Parker, K. J. (**2000**). ''Three-dimensional sonoelastography: Principles and practices,'' Phys. Med. Biol. **45**, 1477–1494.

Yamakoshi, Y., Sato, J., and Sato, T. (**1990**). ''Ultrasonic imaging of internal vibrations of soft tissue under forced vibration,'' IEEE Trans. Ultrason. Ferroelectr. and Freq. Contr., **37**, 45–53.